Title: Wildlife exposure to SARS-CoV-2 across a human use gradient

Running title: Wildlife exposure to SARS-CoV-2

Amanda R. Goldberg[1]*, Kate E. Langwig[1], Jeffrey Marano[2,3], Amanda K. Sharp[4], Katherine L. Brown[5,6], Alessandro Ceci[7], Macy J. Kailing[1], Russell Briggs[7], Clinton Roby[7], Anne M. Brown[5,8,9,10,11], James Weger-Lucarelli[2,6], Carla V. Finkielstein[1,5,6,10,11,12]†*, Joseph R. Hoyt[1]†

[1]Department of Biological Sciences, Virginia Tech, Blacksburg, Virginia, USA
[2]Department of Biomedical Sciences and Pathobiology, Virginia Tech, Blacksburg, Virginia, USA
[3]Translational Biology, Medicine, and Health Graduate Program, Virginia Tech, Roanoke, VA, USA
[4]Program in Genetics, Bioinformatics, and Computational Biology, Virginia Tech, Blacksburg, VA, USA
[5]Virginia Tech Carilion School of Medicine, Virginia Tech, Roanoke, VA, USA
[6]Center for Emerging, Zoonotic, and Arthropod-borne Pathogens, Virginia Tech, Blacksburg, VA, USA
[7]Molecular Diagnostics Laboratory, Fralin Biomedical Research Institute, Virginia Tech, Roanoke, VA, USA
[8]Department of Biochemistry, Virginia Tech, Blacksburg VA, USA
[9]Data Services, University Libraries, Virginia Tech, Blacksburg, VA, USA
[10]Virginia Tech Center for Drug Discovery, Virginia Tech, Blacksburg, VA, USA
[11]Academy of Integrated Science, Virginia Tech, Blacksburg, VA, USA
[12]Integrated Cellular Responses Laboratory, Fralin Biomedical Research Institute at VTC, Roanoke, VA, USA

*Co-corresponding authors: Amanda R. Goldberg, goldberg.amandar@gmail.com; Carla V. Finkielstein, finkielc@vt.edu
†Authors contributed equally

Keywords: Omicron variant, cross-species transmission, spillover, SARS-CoV-2, wildlife

Abstract

The spillover of SARS-CoV-2 into humans has caused one of the most devastating pandemics in recorded history. Human-animal interactions have led to transmission events of SARS-CoV-2 from humans to wild and captive animals. However, many questions remain about how extensive SARS-CoV-2 exposure is in wildlife, the factors that influence wildlife transmission risk, and whether sylvatic cycles can generate novel variants with increased infectivity and virulence. We sampled 18 different wildlife species in the Eastern U.S. and detected widespread exposure to SARS-CoV-2 across wildlife species. Using quantitative reverse transcription polymerase chain reaction and whole genome sequencing, we conclusively detected SARS-CoV-2 in the Virginia opossum and had equivocal detections in six additional species. Species considered human commensals like squirrels, and raccoons had high seroprevalence, ranging between 62%-71%, and sites with high human use had three times higher seroprevalence than low human-use areas. SARS-CoV-2 genomic data from an infected opossum and molecular modeling exposed previously uncharacterized changes to amino acid residues observed in the receptor binding domain (RBD), which predicts improved binding between the spike protein and human angiotensin-converting enzyme (ACE2) compared to the dominant variant circulating at the time of isolation. These mutations were not identified in human samples at the time of collection. Overall, our results highlight widespread exposure to SARS-CoV-2 in wildlife and suggest that areas with high human activity may serve as important points of contact for cross-species transmission. Furthermore, this work highlights the potential role of wildlife in fueling *de novo* mutations that may eventually appear in humans.

Introduction

Severe acute respiratory syndrome coronavirus 2 (SARS-CoV-2), the causative agent of coronavirus disease 2019 (COVID-19), has resulted in over 600 million human cases and over 6 million deaths worldwide (1). As this pathogen becomes endemic in the human population, one of the greatest threats to public health is the resurgence of more transmissible and virulent SARS-CoV-2 variants. The considerable pathogen pressure imposed by the pandemic has caused concern around whether SARS-CoV-2 will spill into wildlife populations and establish a sylvatic cycle. Establishment of SARS-CoV-2 infections in a new host could result in novel mutations that increase virulence, transmissibility, and confer immune escape, which could negatively impact both human and wildlife populations.

Transmission to captive animals has been well documented (2-4), but SARS-CoV-2 detections in free-ranging wildlife are currently limited to only a few species including (5): the white-tailed deer (*Odocoileus virginianus*; (6, 7)), feral mink (*Neovison vison*; (8)) and more recently the Eurasian river otter (*Lutra lutra*; (9)). Experimental infections and modelling of the functional receptor for SARS-CoV-2 (angiotensin-converting enzyme 2: ACE2) have shown several different wildlife taxa may be competent hosts (10, 11). However, which wildlife species are infected in natural settings, where exposure to SARS-CoV-2 is likely to be indirect and at lower exposure dose than in laboratory settings, remains unexplored.

Here we used a combination of quantitative reverse transcription polymerase chain reaction (RT-qPCR) and whole genome sequencing as well as neutralizing antibody surveys to examine wildlife exposure to SARS-CoV-2 along a human-use gradient. We used RT-qPCR on nasopharyngeal swab samples collected from 32 counties in Virginia to detect three distinct SARS-CoV-2 genes (*S, N* and *E*) in conjunction with the amplification of a housekeeping gene from each host to examine active SARS-CoV-2 infection prevalence (12). We assigned positivity based on both amplification of a single viral gene (equivocal detections) as well amplification of two or more genes. At a subset of 6 sites located in Southwest, Virginia (Fig. 1), we quantified the effects of urbanization (percent impervious surface) and human activity on the presence of neutralizing antibodies to SARS-CoV-2 to examine previous exposure along the human-wildlife interface. In addition, we identified unique mutations in SARS-CoV-2 from wildlife and examined them in relation to variants circulating in local communities using whole-genome sequencing (WGS) over the study period. We conducted molecular modeling to predict structural changes that would favor binding to the human ACE2 receptor and promote transmissibility.

Results

We analyzed samples from 333 individuals from 18 species collected across 32 counties in Virginia, U.S. (Table 1, Fig. 1). We conducted more detailed sampling across 11 species (114 samples; Table 1) from 4 counties at 6 sites in Southwestern Virginia, where both nasopharyngeal swabs and serum samples were examined (Fig. S1).

Table 1. Summary of species tested and serology or RT-qPCR results for SARS-CoV-2.

Species	RT-qPCR (n)	Serology (n)	Sero-positive samples	RT-qPCR positive 2 genes[1]	RT-qPCR positive 1 gene[1]
Peromyscus maniculatus	43	14	4		
Procyon lotor	23	11	7		
Didelphis virginiana	64	8	5	1N+S	1N, 3S
Sciurus carolinensis	64	7	5		1S
Peromyscus leucopus	12	6	1		
Mephitis mephitis	10	3	2		
Vulpes vulpes	5				1N
Odocoileus virginianus	10				1S
Lynx rufus	2				1S
Sylvilagus floridanus	69				3N, 1S
Marmota monax	9				
Tamias striatus	8				
Eptesicus fuscus	4				
Blarina brevicada	3				
Lasiurus borealis	3				
Sciurus niger	2				
Mustela vison	1				
Urocyon cinereoargenteus	1				
Total	333	49	24	1	12

[1]Letter denotes SARS-CoV-2 genes(s) that amplified.

Amplification of at least two SARS-CoV-2 genes provided conclusive detections in one sample from a Virginia opossum (*D. virginiana*; (63 individuals), 1.6%; Fig. 1A). Overall active infection prevalence based on just a single gene (*S* or *N*) amplification was ~4% with equivocal detections in 5 additional species. Red fox (*Vulpes vulpes*; 20.0%) and white-tailed deer (*Odocoileus virginianus;* 10.0%) had the highest prevalence, followed by the Virginia opossum (7.8%). Other species with a single gene amplification included the Eastern gray squirrel (*Sciurus carolinensis;* 1.6%), Eastern cottontail rabbit (*Sylvilagus floridanus*; 5.8%), and bobcat (*Lynx rufus;* 50.0%, N=2). Neutralizing antibodies, indicative of prior exposure to SARS-CoV-2, were detected in a much larger number of animals with a total seroprevalence of 48.9%. Antibodies were detected in all species where serum was collected, including the Virginia opossum (62.5%), striped skunk (*Mephitis mephitis*; 66%), raccoon (*Procyon lotor*; 63.6%), Eastern grey squirrel (71.4%), white-footed mouse (*Peromyscus leucopus;* 16.7%) and the deer mouse (*Peromyscus maniculatus*; 28.6%; Fig. 1B).

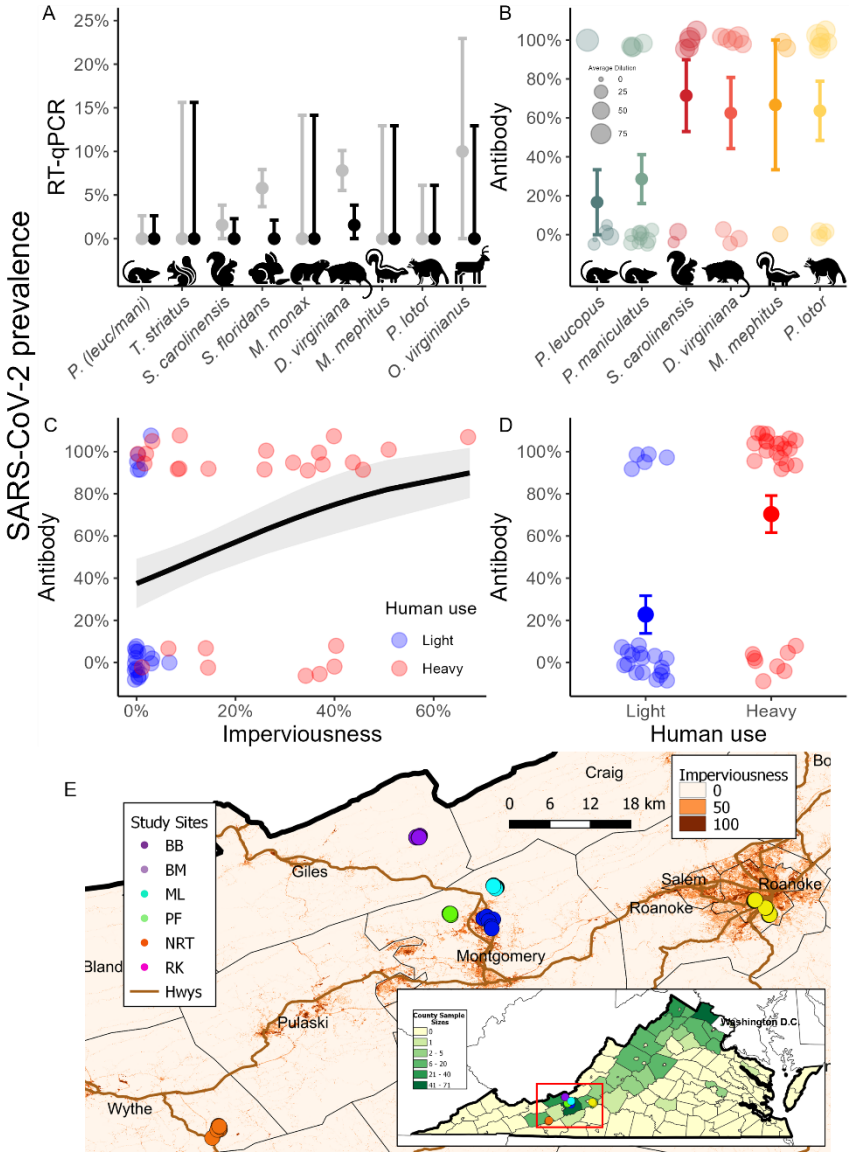

Figure 1. Examination of SARS-CoV-2 exposure across species and the human-wildlife interface. Mean prevalence of (A) RT-qPCR detections and (B) seroprevalence for species sampled. Detections for RT-qPCR include species with >5 individuals sampled and both panels include the prevalence and standard error. Black points in panel (A) represent prevalence based on amplification of two of the three genes (*N*, *S*, and *E*) amplifying at a Cq score under 40. Estimates in gray include samples that amplified just a single gene and had a Cq score <40. The size of each point in panel (B) is in relation to the percent neutralization. Samples with a 50% or greater percent neutralization were considered positive samples. Panel (C) shows the relationship between urbanization (imperviousness) and seroprevalence collected from 5 different sites in VA, USA. The effect of high (~7,000 – 385,000 people/month) and low human use (~10 - 100 people/month) on seroprevalence is represented in panel (D). Error bars and ribbons represent SE. Location of the 6 study sites and counties where viral swabs were collected (E; darker green counties represent larger sample sizes and each colored dot represents one of the 6 study sites where we collected samples in the field). Serology data was collected at 5 of the sites.

We found modest support for a positive relationship between urbanization (imperviousness) and wildlife seroprevalence (intercept: -0.51 ± 0.50, urbanization slope 0.04 ± 0.02, $P = 0.079$, Fig. 1C). Antibody detections were highest (80%) at one of the least urban sites (average imperviousness 1.5%), and more closely matched seroprevalence at two of our urbanized sites (70% and 67%). However, human visitation at this site and other urbanized sites were more than 70x higher compared to the low visitation sites (~7,000-42,000 people/month). Examination of the relationship between human use and seroprevalence of SARS-CoV-2

revealed that high human activity at a site resulted in seroprevalence over 3x higher (intercept: -1.22±0.51, high-use coeff: 2.09±0.66, $P = 0.002$; Fig 1D) than sites with lower human activity (~10-100 people/month).

We conducted WGS of the SARS-CoV-2 variant infecting the opossum which revealed several mutations shared within the Omicron clade as well as unique amino acid substitutions not previously identified in other human-infected SARS-CoV-2 virus at the time of collection (Table 2). The opossum sequence shared defining mutations in *ORF1a*/*b*, *S*, *E*, and *M* genes found in the BA.2 Omicron (Fig. 2).

At the time of the sample collection and genomic analysis, May 2022, we could not confidently assign a variant name. However, more recent phylogenetic analysis of the whole genome showed the isolate clustered within the NextStrain clade 20L (Omicron) and assigned the PANGO lineage BA.2.10.1, also named BJ.1, using UShER (Fig. 2). This Omicron sub-linage includes the $G^{798}D$ mutation found in the Spike protein. The nearest neighbor (EPI_ISL_14334179), which was only recently collected in New York state, and contains all the nucleotide and amino acid mismatches as the opossum sequence versus the reference sequence from Wuhan, China, except for A22974T ($E^{471}V$) that remains unique to the opossum.

Table 2. Summary of mutations identified in the Virginia opossum (*Didelphis virginianus*)

SNP	Gene	Mutation
C7749T	*ORF1ab*/*NSP3*	Missense mutation $T^{2495}I$
T16342C	*ORFab*/*Helicase*	Missense mutation $S^{5390}P$
A20304G	*ORFab*/*EndoRNAse*	Synonymous mutation
A22974T	*S* gene	[1]missense mutation $E^{471}V$
G23955A	*S* gene	[2]missense mutation $G^{798}D$

[1]Fig 2A,[2]Fig. 2A, Sup. Fig. 2A

The $E^{471}V$ mutation is located in the variable receptor-binding motif (RBM, residues 437 to 508) within the receptor-binding domain (RBD, residues 319 to 541) of the S protein. The RBD is necessary for binding the viral protein to ACE2 in both human and animal cells and is, in addition, therapeutically targeted by neutralizing monoclonal antibodies (13).

We performed a detailed computational investigation into the impact of the $E^{471}V$ and $G^{798}D$ mutations for the structure of the S protein using molecular modelling and molecular mechanics/generalized borne surface area (MM/GBSA) free energy calculations. The open conformation structure of S protein trimer from the glycosylated BA.2 Omicron variant was used for residue variant mapping [PDB 7XO8; (14)]. Because the crystal structure shows the trimer bound to the human ACE2 (hACE2) receptor, it is possible to investigate the impact of mutations in the hACE2 RBD and predict favorable interactions between SARS-CoV-2 S protein and

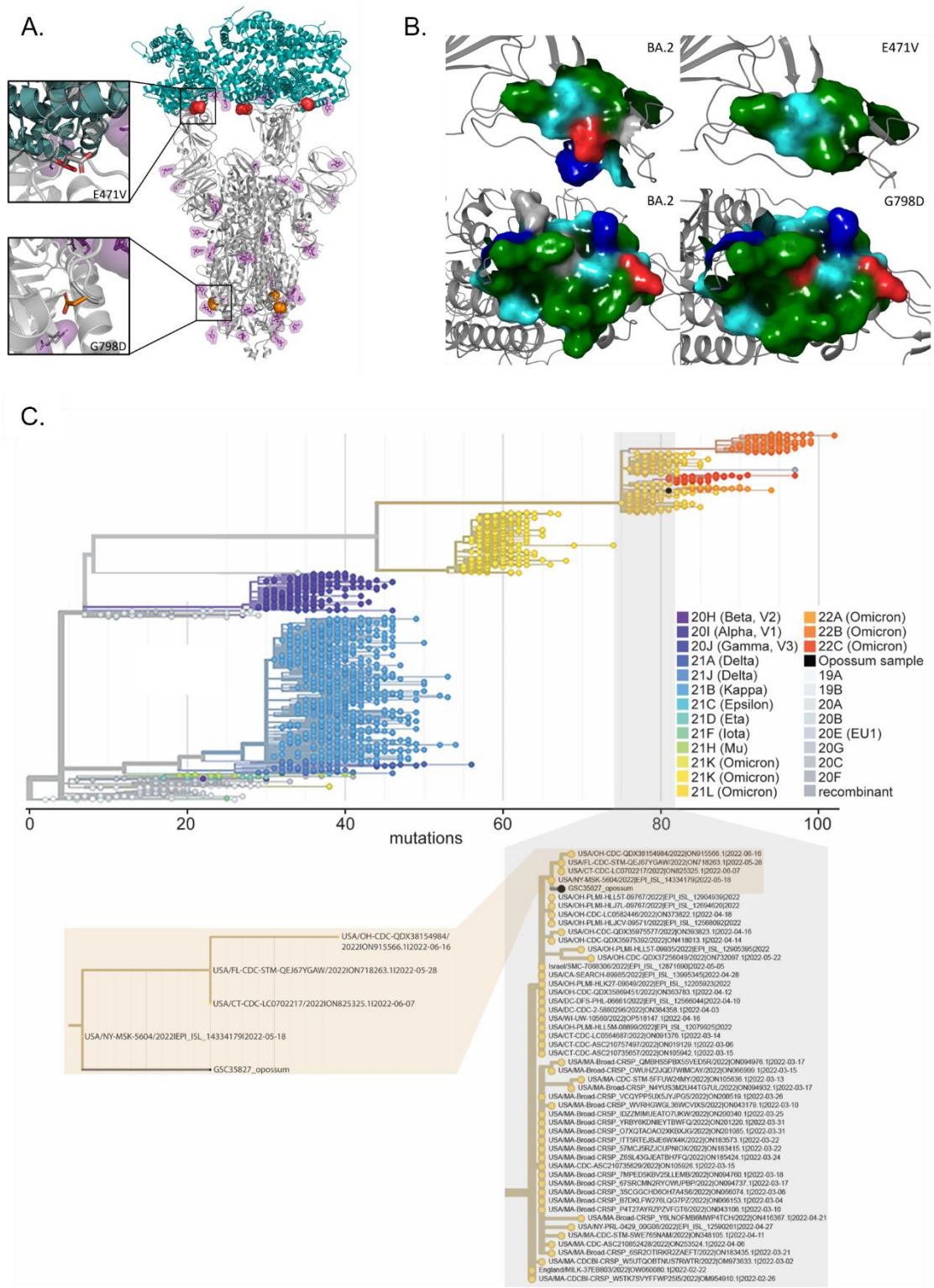

Figure 2. Molecular modeling of unique S mutations and Whole Genome Sequencing of the Virginia opossum SARS-CoV-2 virus. (A) Representation of the structure of the BA.2 S protein (gray, PDB: 7XO8) in its open conformation bound to the human ACE2 (teal). Residues 471 (red) and 798 (orange) are shown as spheres. Glycans are displayed as sticks colored purple. Top inset: Overlay of $E^{471}V$ (red) and BA.2 (grey). Bottom inset: Overlay of $G^{798}D$ (orange) and BA.2 (grey). (B) Surface map of the BA.2 S protein (left) and the region surrounding $E^{47}1V$ and

$D^{798}G$ (right) residues. Residue side chain properties are colored: green for hydrophobic, blue for positively charged, red for negatively charged, teal for polar uncharged, and gray for neutral. (D) Global phylogenetic tree using 2,001 sequences including the opossum SARS-CoV-2 whole genome sequence is shown clustering within the NextStrain clade 20L (Omicron). Subtrees show the placement of the opossum SARS-CoV-2 sequence within the 20L cluster in more detail.

hACE2 as previously reported (15) (Fig. 2). Our free energy studies showed predicted free energy of binding between the $E^{471}V$-carrying mutation in S improved, compared to that of BA.2, for binding to hACE2 (-76.5 and -60.2 kcal/mol for E471V vs. BA.2, respectively). Residue 471 is predicted to be part of a flexible, hydrophobic loop that interacts with the N-terminal domain of ACE2 (Fig. 2). Several point mutations ($A^{475}V$, $S^{477}G$, $V^{483}A$, $F^{490}L$) within this loop region have experimentally shown to improve S protein – hACE2 binding affinity and increased resistance to neutralizing antibodies (16, 17), suggesting increased evolutionary pressure to create a more flexible, hydrophobic surface. Our analysis using normalized Kyte-Doolittle hydropathy scores and surface maps show a more hydrophobic interaction surface at not just position 471, but also among flanking residues 469-474 (0.8) compared to BA.2 [-2.6; (18)].

We located a second missense mutation, $G^{798}D$, in the S2 subunit of the S protein (residues 686 to 1,273) and within the fusion peptide domain (residues 788 to 806) in close proximity to the N^{801} glycosylation site. Interestingly, D^{798} changed the probability of glycosylation at N^{801} (0.48) as compared to BA.2 [0.61, (19)] and could impact structural stability and membrane interaction (20) (Fig. 2 and Fig. S3).

Discussion

We found that exposure to SARS-CoV-2 appears widespread among wildlife species. We detected positives in 6 species using RT-qPCR and neutralizing antibodies in an additional 4 species. We found support for a relationship between human use and seroprevalence suggesting that areas with high human activity are potential hotspots for cross-species transmission. Analysis of isolates collected from infected wildlife revealed novel mutations at the time of collection which have subsequently been found circulating in other regions. While some of these mutations likely increase binding affinity to the hACE2 receptor or confer some antibody resistance compared to ancestral BA.2 lineages, others appeared unique to the opossum. Whether these mutations developed in humans not captured in surveillance at the time or in wildlife communities and were transmitted back to humans remains unknown but presents an important consideration for future variant surveillance.

Our combined results suggest that a high diversity of species are exposed to SARS-CoV-2 in the wild. Prevalence of active infections among wildlife was generally low and ranged from 1.6-20.0%. We found that 7.8% of opossums, a marsupial, were positive (including equivocal detections), similar to white-tailed deer (10.0%). High seroprevalence (62%) and a single opossum with viral RNA levels at sufficient levels for WGS suggests this species may have high exposure to SARS-CoV-2 in natural settings. The SARS-CoV-2-positive opossum with two gene amplification was recaptured at the same site ~30 days later, and was positive for antibodies

(51.1 % neutralization), supporting that the serology data reflect previous infection with SARS-CoV-2. The Eastern gray squirrel also had detections on both RT-qPCR (1.6%) and using serological tests (71.4%). Several other species that were examined for antibodies to SARS-CoV-2 suggested high levels of previous exposure, including raccoons (64%) and skunks (67%). All these species are considered human commensals and live in and around human settlements. Many of these species' range across large areas of North America and some have been introduced into Europe (gray squirrel and raccoon) and Asia (raccoon) and have close relatives across the globe. While it is unknown whether a sylvatic cycle has been established in any of these species, their close connection to human populations makes them important species for considering transmission to and from humans.

We found a relationship between human use, urbanization and seroprevalence among sites. This suggests that wildlife in areas with more human activity likely have higher exposure to SARS-CoV-2, leading to more wildlife infections. Interestingly, the site with the highest seroprevalence was a forested recreational trail that receives high human visitation but is less developed. This suggests that recreational sites may be important points of contact between humans and wildlife and could be targeted for surveillance. Humans and wildlife rarely come into direct contact, but numerous indirect links likely exist. Wastewater has been proposed as a potential source for indirect exposure to SARS-CoV-2 (21), however, in rural areas where septic tanks are a dominant form of wastewater management, this is unlikely to be the only source. Instead, other forms of human waste, like trash receptacles, may serve as important sources of indirect exposure for wildlife (22, 23).

SARS-CoV-2 isolated from the opossum, showed unique mutations in the spike protein in the RBM and RBD of the spike protein. These previously uncharacterized amino acid changes are predicted to improve S-hACE2 binding and membrane fusion efficiencies compared to omicron BA.2, potentially providing a fitness advantage by either increasing the affinity of S for the ACE2 receptor or, alternatively, by evading the neutralizing activity of antibodies. These mutations were not observed in human samples at the time of isolation from the opossum and have only recently been identified in a new Omicron sub-variant (BJ.1). These results highlight the role of wildlife in contributing unique mutations that may be more transmissible to humans as has been previously suggested with the emergence of the Omicron variant (6, 24)

Methods

Wildlife were sampled using nasopharyngeal and/or oropharyngeal swabs through active captures as well as through submissions to wildlife centers. At six sites we actively trapped wildlife using live-traps from May through July, 2022. Sites were trapped 3-4 nights each depending on animal activity. We anesthetized and swabbed all animals, and collected blood from a subset of individuals. Urbanization was calculated as the percent of impervious surface and adjusted based on the home range of each species captured and human activity was estimated based on trail counters, visitation records or extrapolated from census data. We used generalized linear mixed models to evaluate relationships between seroprevalence and human use and urbanization (See Supplemental Methods). This study was performed under Virginia Tech IACUC protocol #22-061.

Samples were RT-qPCR tested using our Emergency Use Authorized SARS-CoV-2 assay (12). Samples were reported conclusively positive when 2/3 SARS-CoV-2 genes (*N*, *E*, and *S*) and the housekeeping gene (*CYCS* for wildlife) amplified below the threshold established by corresponding standard curves (12). We did a full phylogenetic sequencing of SARS-CoV-2 from the opossum and conducted molecular modeling as indicated in Supplemental Methods. We used a plaque reduction neutralization test (PRNT) with a SARS-CoV-2 GNL-1205 stock. We categorized serum samples as positive if they had at least a 50% neutralization at a 1:20 dilution and negative if they had less than a 50% neutralization.

Author contributions

A.R.G., K.E.L., and J.R.H. designed field research; A.R.G., M.J.K, and K.E.L performed field research; J.M, K.E.L., J.W, C.R, A.C., R.B., C.V.F., and J.R.H. contributed to field data analysis; A.K.S., A.B., K.B., and C.V.F contributed to molecular analysis; K.E.L., J.W., C.V.F., and J.R.H. provided project administration; Members of the Molecular Diagnostics Laboratory provided technical support; and all authors aided in interpreting results and to writing the paper.

Acknowledgements

We thank the following for land access: J Eustis and New River Land Trust; B Brodie, J Jones and Mountain Lake Biological Research Station; R Powers, K Slusher, A McGee and Roanoke Parks and Recreation; V Malzone, G Gorecki, S Sweeney, J Elliott, and Virginia State Parks; G O'Malley, A Lewis, H Wander, K Malewicz, V Corbin, R Cohen, S Whitehead and family, N Laggan, A Grimaudo, and G Blanvillain. We thank the following for help with study design and collection: M Fisher, J Ivan, K Bentler, S Yamada, C Cereghino, K Pierce and the Wildlife Center of Virginia, J Riley and the Blue Ridge Wildlife Center, and H Olsen-Hodges and the Southwest Virginia Wildlife Center. This project was supported by Virginia Tech and funds from the Fralin Biomedical Research Institute to C.V.F. and a One Health award from VCOM to J.W.

Data Availability

All study data are included in the article and supporting information. Sequence data from SARS-CoV-2 viruses from Virginia opossum sequenced in this study are available in the GISAID database (https://www.gisaid.org/) and NCBI (https://ncbi.nlm.nih.gov) SARS-CoV-2 sequence repositories.

References

1. World Health Organization (2020) WHO COVID-19 Dashboard. (Geneva).
2. M. Drozdz *et al.*, Current State of Knowledge about Role of Pets in Zoonotic Transmission of SARS-CoV-2. *Viruses-Basel* **13**, 1149 (2021).
3. M. Fritz *et al.*, High prevalence of SARS-CoV-2 antibodies in pets from COVID-19+ households. *One Health* **11**, 100192 (2020).
4. H. L. Murphy, H. Ly, Understanding the prevalence of SARS-CoV-2 (COVID-19) exposure in companion, captive, wild, and farmed animals. *Virulence* **12**, 2777-2786 (2021).

5. G. Pappas, D. Vokou, I. Sainis, J. M. Halley, SARS-CoV-2 as a Zooanthroponotic Infection: Spillbacks, Secondary Spillovers, and Their Importance. *Microorganisms* **10**, 2166 (2022).
6. V. L. Hale *et al.*, SARS-CoV-2 infection in free-ranging white-tailed deer. *Nature* **602**, 481-486 (2022).
7. J. C. Chandler *et al.*, SARS-CoV-2 exposure in wild white-tailed deer (*Odocoileus virginianus*). *P Natl Acad Sci USA* **118**, e2114828118 (2021).
8. J. Aguiló-Gisbert *et al.*, First description of SARS-CoV-2 infection in two feral American mink (*Neovison vison*) caught in the wild. *Animals* **11**, 1422 (2021).
9. M. Padilla-Blanco *et al.*, The finding of the severe acute respiratory syndrome coronavirus (SARS-CoV-2) in a Wild Eurasian River Otter (*Lutra lutra)* highlights the need for viral surveillance in wild mustelids. *Front Vet Sci* **9** (2022).
10. F. Martínez-Hernández *et al.*, Assessing the SARS-CoV-2 threat to wildlife: Potential risk to a broad range of mammals. *Perspectives in ecology and conservation* **18**, 223-234 (2020).
11. D. A. Meekins, N. N. Gaudreault, J. A. Richt, Natural and Experimental SARS-CoV-2 Infection in Domestic and Wild Animals. *Viruses-Basel* **13**, 1993 (2021).
12. A. Ceci *et al.*, Development and implementation of a scalable and versatile test for COVID-19 diagnostics in rural communities. *Nature Communications* **12**, 1-14 (2021).
13. P. C. Taylor *et al.*, Neutralizing monoclonal antibodies for treatment of COVID-19. *Nat. Rev. Immunol.* **21**, 382-393 (2021).
14. Z. Xu *et al.*, Integrated strategy of RNA-sequencing and network pharmacology for exploring the protective mechanism of Shen-Shi-Jiang-Zhuo formula in rat with non-alcoholic fatty liver disease. *Pharm Biol* **60**, 1819-1838 (2022).
15. Y. F. Kang *et al.*, Rapid Development of SARS-CoV-2 Spike Protein Receptor-Binding Domain Self-Assembled Nanoparticle Vaccine Candidates. *Acs Nano* **15**, 2738-2752 (2021).
16. V. Singh *et al.*, Stroke increases the expression of ACE2, the SARS-CoV-2 binding receptor, in murine lungs. *Brain Behav Immun* **94**, 458-462 (2021).
17. H. D. Li *et al.*, Greener liquid-phase synthesis and the ACE inhibitory structure-activity relationship of an anti-SARS octapeptide. *Org Biomol Chem* **18**, 8433-8442 (2020).
18. H. Beard, A. Cholleti, D. Pearlman, W. Sherman, K. A. Loving, Applying Physics-Based Scoring to Calculate Free Energies of Binding for Single Amino Acid Mutations in Protein-Protein Complexes. *Plos One* **8**, e82849 (2013).
19. M. Huang *et al.*, Atlas of currently available human neutralizing antibodies against SARS-CoV-2 and escape by Omicron sub-variants BA.1/BA.1.1/BA.2/BA.3. *Immunity* **55**, 1501-1514 (2022).
20. A. Shajahan, L. E. Pepi, D. S. Rouhani, C. Heiss, P. Azadi, Glycosylation of SARS-CoV-2: structural and functional insights. *Analytical and Bioanalytical Chemistry* **413**, 7179-7193 (2021).
21. A. B. Franklin, S. N. Bevins, Spillover of SARS-CoV-2 into novel wild hosts in North America: A con- ceptual model for perpetuation of the pathogen. *Sci. Total Environ.* **733**, 139358 (2020).
22. R. Francisco *et al.*, Experimental Susceptibility of North American Raccoons (Procyon lotor) and Striped Skunks (Mephitis mephitis) to SARS-CoV-2. *Front Vet Sci* **8**, 10 (2022).
23. J. Han *et al.*, Municipal solid waste, an overlooked route of transmission for the severe acute respiratory syndrome coronavirus 2: a review. *Environ. Chem. Lett.*, 1-15 (2022).

24. S. V. Kuchipudi *et al.*, Multiple spillovers from humans and onward transmission of SARS-CoV-2 in white-tailed deer. *P Natl Acad Sci USA* **119**, e2121644119 (2022).

Extended Methods

Trapping and processing

We collected nasopharyngeal or oropharyngeal samples from wildlife across 32 counties in Virginia, U.S.A. We collected samples from 3 wildlife rehabilitation centers in Boyce, Roanoke, and Waynesboro, VA In addition, we actively captured wildlife from 6 sites that spanned a rural to urban gradient in Giles, Montgomery, Roanoke, and Wythe counties (Table S1, Fig. S1).

We trapped each site for a 2-4 day session, and used 3 different sized live traps to capture animals: Tomahawk non-folding traps (Tomahawk Live Trap Co., Tomahawk, WI, U.S.A; 46 x 15 x 15cm, model 103.5), Tomahawk folding traps (66 x 23 x 23cm, model 205 or 81 x 25 x 31, model 207), and Sherman folding traps for smaller animals (Sherman Traps, Tallahassee, FL, U.S.A; 8 x 9 x 23cm, model LFG). We set and baited traps in the evening just before dark and checked them the following morning before 10:00 AM to ensure animals did not get overheated. The study was performed under the Virginia Tech IACUC protocol #22-061.

We processed all animals in the area where they were trapped. We anesthetized larger animals in either a bucket chamber (1) or in a 50L clear box chamber (58 x 38 x 56 cm, Fig. S4). We used a tec-4 funnel fill with a cage mount manifold vaporizer (Ohmeda, West Yorkshire, UK) connected to a portable medical oxygen cylinder (size E) with a built-in regulator (Walk-02-Bout+^{TM}, Airgas Healthcare, Radnor, PA). We used a 2 L/min oxygen mix to 3-4% isoflurane mix in the chambers. Smaller animals were placed in a small plastic canister and anesthetized with 0.5 – 1.2mL isoflurane (dosage depended on species and body size), placed onto a cotton ball to prevent direct contact with the animal. Once anesthetized, we removed animals from the chamber, and then masked animals (mice were only masked for collecting serum samples; Fig S4) with a dose of 2 L/min oxygen and 2-3% isoflurane.

We marked individuals with aluminum ear tags in each ear (National Band and Tag Company, model 1005-1 or 1005-3 depending on body size). We collected morphometric, sex and reproductive status from each animal. For RT-qPCR detections, we swabbed each individual with a polyester swab (25-800 1PD swab for larger mammals and 25-1000 1PD swab for smaller animals (juveniles, skunks, squirrels, bats, shrews, and mice); Puritan Medical Products, Guilford, ME, U.S.A). We used an oropharyngeal swab for animals that were too small for nasopharyngeal swabbing (mice, shrews, bats, etc.). We collected blood for antibody screening from the submandibular vein for mice and from the nail quick of one of the rear toe nails for all other species. Blood was stored in microvette 500 z-gel tubes for later processing. All field personnel wore N95 masks and gloves to reduce transmission between humans and wildlife.

Urbanization and human use variables

We obtained estimates of urban imperviousness from the National Land Cover Database 2019 (2, 3). We obtained estimates of population density from 2020 census at the 30 sec spatial scale (4). We created buffers of variable sizes based on species home range size to calculate the mean estimates of imperviousness and population density for each individual capture location (Table S2). We established two land use categories: low (fewer than 500 people using the local landscape per month) and high (500 or more people using the landscape per month). Estimates of human activity at each of the sites were provided by the organizations managing the land or population estimates (Table S1).

We obtained estimates of human use at the 5 sites where we collected serology data (Table S1). New River Trails State Park and Roanoke Parks and Recreation provided monthly

human visitation estimates between March and August 2022. Mountain Lake Biological Research Station provided us an estimate for how many people were using the facilities at the station between March and August 2022; they averaged about 50 people at the station per month and we multiplied it by 7 (1 week) to represent that each person may have stayed ~7 days. Brush Mountain recreational area was closed to the public from March through August 2022 so we assumed approximately 10 people used the area per month. For the town of Blacksburg, we used population estimates from the 2020 census (TIGER/Line, U.S. Census Bureau, 2020 Blocks). We created a minimum convex polygon (mcp) in the adehabitatHR package (5) in program R around the different trapping locations. We then calculated the population for each census block by multiplying the percent of the block within the mcp by the population count. We then summed the population within the mcp to estimate the total population. We multiplied the population count by 30 to estimate the number of people per month using that area.

Statistical Analyses

We used the sf (6) and exactextractr (7) packages in program R v 4.1.1 (8) to calculate the mean of the urbanization variables within each of our trap buffers. We used the glmmTMB package (9) in program R to analyze generalized linear mixed models to assess whether seroprevalence rates were impacted by the following covariates: urbanization (imperviousness), population density, and species and included site as a random effect. We used Akaike information criterion corrected for small sample sizes (AICc) for model selection (10) to evaluate the fit of 6 models and considered any with a delta AICc < 2.0 to have support. Additionally, we ran a generalized linear mixed model (GLMM) with the human use grouping variables (high vs low) and included species as a random effect.

Sample testing

We carried out nucleic acid purification and amplification of SARS-CoV-2 using our Emergency Use Authorized SARS-CoV-2 assay as previously described with a few specific modifications [Federal Drug Administration, (11)]. Briefly, we processed swab-containing media shortly after collection and total RNA purified using 96-well spin columns, assessed for quality control, and subjected to synthesis and amplification using the Power SYBR™ Green RNA-to-CT™ 1-Step kit (Applied Biosystems). Our in-house test detects multiple targets including the nucleocapsid (*N*), envelope (*E*), and spike (*S*) genes of the SARS-CoV-2 virus, as well as the cytochrome c (*CYCS*) housekeeping gene for which species-specific primers were designed (Table S3). RT-qPCR reactions were performed in a CFX384 Touch Real-Time PCR Detection System (Bio-Rad), positive control using inactive SARS-CoV-2 virus (ATCC®), no template controls, and standard curves were included in each plate as previously described (11).

Whole genome sequencing and Sanger amplification

To amplify the entire SARS-CoV-2 genome, positive samples were reverse transcribed and amplified using SuperScript IV Reverse Transcriptase (Thermofisher) and ARTIC nCoV-2019 Amplicon Panel V4.1 primers (Integrated DNA technologies). Purified PCR products were barcoded using the plexWell™ 384 Library Preparation Kit (seqWell, MA) and the pooled library sequenced using a MiSeq System (Illumina, CA)

following manufacturer's instructions. SARS-CoV-2 sequencing analysis was accomplished using an established pipeline and optimized workflow for validation that combines tools to assess quality, sequence alignment, variation calling, and variant assignment. Lineage assignments were processed using Pangolin software suite (https://cov-lineages.org/) (12). Whole genome sequences were deposited in the GISAID database (https://www.gisaid.org/) and NCBI (https://ncbi.nlm.nih.gov) SARS-CoV-2 sequence repositories.

Phylogenetic analysis

A FASTA file containing the opossum SARS-CoV-2 whole genome sequence was uploaded in Ultrafast Sample placement on Exiting tRee [UShER; https://genome.ucsc.edu/cgi-bin/hgPhyloPlace, (13, 14)] for global phylogenetic tree analysis using 12,397,869 SARS-CoV-2 genomes obtained from GISAID, GenBank, COG-UK and CNCB that were available as of 2022-10-03. The resulting global tree and subtree were visualized using NextStrain's interactive display [https://nextstrain.org/, (15)] and 2001 and 50 sequences, respectively.

Molecular modeling

Computational studies were carried out using the structure of the glycosylated Omicron BA.2 variant bound to the human ACE2 receptor [Protein Data Bank 7XO8; (16)]. We incorporated point mutations in BA.2 using PyMOL (The PyMOL Molecular Graphics System v. 2.4.0, Schrödinger, LLC) to generate a new structure containing both E471V and G798D mutations. We then performed energy minimization using Schrödinger-Maestro (v. 2020.4) and OPLS3e force field (17, 18). We used Schrödinger Bioluminate to carry out molecular mechanics/generalized borne surface area (MM/GBSA) energy calculations (19, 20) as well as surface mapping [v. 2020.4; (21)]. Glycosylation propensity was calculated using the NetNGlyc 1.0 server (22).

Genomic data

Human (13,221) and wildlife (333) clinical samples were analyzed for the presence of SARS-CoV-2 by RT-qPCR as described in the Materials and Methods section. Samples were considered conclusively positive when 2 of 3 SARS-CoV-2 genes (*N*, *E*, and *S*) and the housekeeping gene (*RPP30* for humans and *CYCS* for wildlife) amplified below the threshold established by corresponding standard curves (11). We performed whole genome and amplicon sequencing for conclusively positive samples (Fig. 1A). We limited the description of variants in the human population to the window at which wild sample collection took place (May 1, 2022 to September 8, 2022).

The analysis of human clinical specimens identified 4, 123, 8, 350, 162, 586 as positive, negative, inconclusive, or invalid (no housekeeping gene detected), respectively (Fig. S1A). All positive samples with Cq values <33 were sequenced and have a variant assignment. A few samples failed sequencing or were not assigned due to their quality/quantity and low sequence depth. As shown in Sup. Fig. S1B, various SARS-CoV-2 lineages expanded the window of our study with BA.1 (0.17%), BA.2 (15.85%), BA.2.12.1 (25.80%), BA.4 (14.83%), BA.5 (37.91%), BE (1.57%), BF (1.45%), BG.2 (0.05%), AY.103 (0.02%), no assigned (N/A, 2.24%) being the most prevalent among humans in the region.

Serology data

Serum samples were heat inactivated at 55°C for 1 hour. We serially diluted the serum samples in RPMI-1640 with 10 mM HEPES and 2% FetalPure bovine serum (Genesee Scientific 25-525H). Serum samples were mixed with 1300 plaque-forming units per mL (PFU/mL) of SARS-CoV-2 GNL-1205. The mixture was then incubated at 37°C for one hour, and then the virus-serum mixture was used to inoculate wells in a confluent 24-well plate of VeroE6 hACE2-TMPRSS2 cells. After a one-hour adsorption period, we added plaque assay overlay media to each well, as previously described (23). Based on previously published serosurveillance studies (24-27), we used the following testing criteria:

1. ≥ 90 % Neutralization at a 1:20 Dilution – Strong Positive
2. ≥ 50 % Neutralization at a 1:20 Dilution – Weak Positive
3. < 50 % Neutralization at 1:20 Dilution – Negative

We then ultimately decided to count any individual with at least a 50% Neutralization as positive to analyze the effects of urbanization and human use on SARS-CoV-2 exposure.

References Cited

1. K. T. Bentler, D. N. Gossett, J. J. Root, A novel isoflurane anesthesia induction system for raccoons. *Wildlife Society Bulletin* **36**, 807-812 (2012).
2. J. Dewitz, U.S. Geological Survey National Land Cover Database (NLCD) 2019 Products. Deposited 2021.
3. J. Wickham, S. V. Stehman, D. G. Sorenson, L. Gass, J. A. Dewitz, Thematic accuracy assessment of the NLCD 2016 land cover for the conterminous United States. *Remote Sens Environ* **257**, 112357 (2021).
4. C. C. U. Center for International Earth Science Information Network, *Gridded Population of the World, Version 4 (GPWv4): Population Density, Revision 11* (NASA Socioeconomic Data and Applications Center (SEDAC), Palisades, New York, 2018).
5. C. Calenge, The package "adehabitat" for the R software: A tool for the analysis of space and habitat use by animals. *Ecol Model* **197**, 516-519 (2006).
6. E. Pebesma, Simple Features for R: Standardized Support for Spatial Vector Data. *R J* **10**, 439-446 (2018).
7. D. Baston (2020) exactextractr: Fast extraction from raster datasets using polygons. in *R package version 0.5. 0*.
8. R. C. Team (2021) R: A Language and Environment for Statistical Computing. (R Foundation for Statistical Computing, Vienna, Austria).
9. M. E. Brooks *et al.*, glmmTMB balances speed and flexibility among packages for zero-inflated generalized linear mixed modeling. *The R journal* **9**, 378-400 (2017).
10. K. P. Burnham, D. R. Anderson, K. P. Huyvaert, AIC model selection and multimodel inference in behavioral ecology: some background, observations, and comparisons. *Behavioral ecology and sociobiology* **65**, 23-35 (2011).
11. A. Ceci *et al.*, Development and implementation of a scalable and versatile test for COVID-19 diagnostics in rural communities. *Nature Communications* **12**, 1-14 (2021).
12. A. O'Toole *et al.*, Assignment of epidemiological lineages in an emerging pandemic using the pangolin tool. *Virus Evol* **7** (2021).
13. P. Sagulenko, V. Puller, R. A. Neher, TreeTime: Maximum-likelihood phylodynamic analysis. *Virus Evol* **4** (2018).
14. Y. Turakhia *et al.*, Ultrafast Sample placement on Existing tRees (UShER) enables real-time phylogenetics for the SARS-CoV-2 pandemic. *Nat Genet* **53**, 809-816 (2021).

15. J. Hadfield *et al.*, Nextstrain: real-time tracking of pathogen evolution. *Bioinformatics* **34**, 4121-4123 (2018).
16. Z. Xu *et al.*, Integrated strategy of RNA-sequencing and network pharmacology for exploring the protective mechanism of Shen-Shi-Jiang-Zhuo formula in rat with non-alcoholic fatty liver disease. *Pharm Biol* **60**, 1819-1838 (2022).
17. E. Harder *et al.*, OPLS3: A Force Field Providing Broad Coverage of Drug-like Small Molecules and Proteins. *J Chem Theory Comput* **12**, 281-296 (2016).
18. D. Shivakumar *et al.*, Prediction of Absolute Solvation Free Energies using Molecular Dynamics Free Energy Perturbation and the OPLS Force Field. *J Chem Theory Comput* **6**, 1509-1519 (2010).
19. M. P. Jacobson, R. A. Friesner, Z. X. Xiang, B. Honig, On the role of the crystal environment in determining protein side-chain conformations. *J Mol Biol* **320**, 597-608 (2002).
20. M. P. Jacobson *et al.*, A hierarchical approach to all-atom protein loop prediction. *Proteins* **55**, 351-367 (2004).
21. H. Beard, A. Cholleti, D. Pearlman, W. Sherman, K. A. Loving, Applying Physics-Based Scoring to Calculate Free Energies of Binding for Single Amino Acid Mutations in Protein-Protein Complexes. *Plos One* **8**, e82849 (2013).
22. K. Julenius, NetCGlyc 1.0: prediction of mammalian C-mannosylation sites. *Glycobiology* **17**, 868-876 (2007).
23. J. L. Liu *et al.*, Stabilization of a Broadly Neutralizing Anti-Chikungunya Virus Single Domain Antibody. *Front Med (Lausanne)* **8**, 626028 (2021).
24. A. M. Bosco-Lauth *et al.*, Experimental infection of domestic dogs and cats with SARS-CoV-2: Pathogenesis, transmission, and response to reexposure in cats. *Proceedings of the National Academy of Sciences* **117**, 26382-26388 (2020).
25. A. M. Bosco-Lauth *et al.*, Susceptibility of livestock to SARS-CoV-2 infection. *Emerging Microbes & Infections* **10**, 2199-2201 (2021).
26. S. A. Shriner *et al.*, SARS-CoV-2 Exposure in Escaped Mink, Utah, USA. *Emerg Infect Dis* **27**, 988-990 (2021).
27. P. M. Palermo, J. Orbegozo, D. M. Watts, J. C. Morrill, SARS-CoV-2 Neutralizing Antibodies in White-Tailed Deer from Texas. *Vector Borne Zoonotic Dis* **22**, 62-64 (2022).

Table S1. Estimates of monthly human use at the 5 sites we trapped and collected serological data. We then grouped the estimates into two categories: High human use (≥500 people per month) or low human use (<500 people per month).

Site	County	Monthly Use Estimates	Human Use Group
Mountain Lake Biological Station	Giles	350	Low
Brush Mountain	Montgomery	10	Low
Blacksburg	Montgomery	384,540	High
Roanoke Parks	Roanoke	79,324	High
New River Trails State Park – Foster Falls	Wythe	57,712	High

Table S2. Buffer width set for use to estimate imperviousness and population density. Buffer width differed by species to represent the space used by each individual trapped.

Species	Buffer width (m)	Source
Peromyscus spp.	50	Wolff, J. O. 1985. The effects of density, food, and interspecific interference on home range size in *Peromyscus leucopus* and *Peromyscus maniculatus*. Canadian Journal of Zoology 63:2657-2662.
Sciurus carolinensis	225	Koprowski, J. L., K. E. Munroe, and A. J. Edelman. 2016. Gray not grey: Ecology of Sciurus carolinensis in their native range in North America. The Grey Squirrel: ecology & management of an invasive species in Europe. Woodbridge, Suffolk UK: European Squirrel Initiative, 1-18.
Didelphis virginiana	500	Gallo, T., et al. 2022. Mammals adjust diel activity across gradients of urbanization. Elife 11:e74756.
Mephitis mephitis	1000	Gallo, T., et al. 2022. Mammals adjust diel activity across gradients of urbanization. Elife 11:e74756.
Procyon lotor	1000	Gallo, T., et al. 2022. Mammals adjust diel activity across gradients of urbanization. Elife 11:e74756.

Table S3. Housekeeping primer sequences for RT-qPCR testing in 18 wildlife species for presence of SARS-CoV-2

Species	Gene/Primer Name	Seq ref	Forward	Revers
Blarina brevicauda	COI-1	NC_042734.1	GCCAACTCATCTCTGGACATTG	ATCCTGCAATGATGGCGAATAC
Didelphis virginiana	COI-2	NC_001610.1	TTGAGAAGCTTTCGCATCCAAAC	GGAGGTGGGCATCCGTATAATC
Eptesicus fuscus	COI-1	MF143474.1	CCTGACGCCTATACAACCTGAAA	GGACGCAAAGGCTTCTCATACTA
Lasiurus borealis	COI-1	NC_016873.1	GGCTTCCGTCGATCTGACTATTT	ATTGAGATAGTGCGGGAGGTTT
Lynx Rufus	COI-1	NC_014456.1	GATGTAGACACACGAGCATACTTTAC	GGCGGGAGACCATTTGATATTG
Marmota monax	COI-1	LR632920.1	ACCGCCTGCCATATCTCAATAC	CTGCTGCAAGAACTGGAAGAGA
Marmota monax	COI-2	LR632920.1	CAGGTGCAGGAACAGGATGAA	CCTGCTAAGTGAAGGGAGAAGATAG
Mephitis mephitis	COI-2	NC_020648.1	ACTGTGAGCACTAGGGTTCATTT	CGTGGAGTACAATATCCAGTGAGG
Mustela vison	COI-1	AY377152.1	ACCTCCCGCTATATCACAATACC	GCTAGGACTGGCAAGGATAGAA
Odocoileus virginianus	COI-1	NC_015247.1	CAGGGACAGGCTGAACTGTTTAT	CACCCGCCAAGTGTAGAGAAA
Peromyscus leucopus	COI-1	NC_037180.1	TGACTACTACCTCCCTCATTCCTC	CAGCTAAGGGTGGGTATACAGTTC
Peromyscus maniculatus	COI-1	JN312100.1	TGACTACTACCTCCCTCATTCCTC	CAGCTAAGGGTGGGTATACAGTTC
Procyon lotor	COI-1	NC_009126.1	CACCGCTCTCAGCCTACTAATTC	AGCATGGGCAGTTACGATTACA
Sciurus carolinensis pennsylvanicus	COI-1	NC_050012.1	TTGGTGGCTTTGGGAATTGATTAG	AGGAGGAAGGAAGGAGGTAGAA
Sciurus niger	COI-1 Scriurus carolinensis pennsylvanicus			
Sylvilagus floridanus	COI-1	JF443513.1	AGGGACAGGCTGAACTGTTTAC	ACTCCGGCTAAGTGAAGAGAGA
Tamias striatus	COI-1	NC_032375.1	ACCACCTACCTATGTTCATCAATCG	CATTCCTGCTCAAGCACCAAATAG
Urocyon cinereoargeneus	COI-1	NC_026723.1	CCCTGCTATATCTCAGTACCAAACTC	GCCAACACGGGTAGTGATAGAA
Vulpes vulpes	COI-1	NC_008434.1	CACTGCCCTAAGCCTCCTAATTC	AGGCATGTGCGGTTACGATTA
Vulpes vulpes	COI-3	NC_008434.1	ACCGCACATGCCTTCGTAATA	ATCCGAGGAAATGCTATGTCTGG

[1]COI=CytochromeC oxidase subunit1

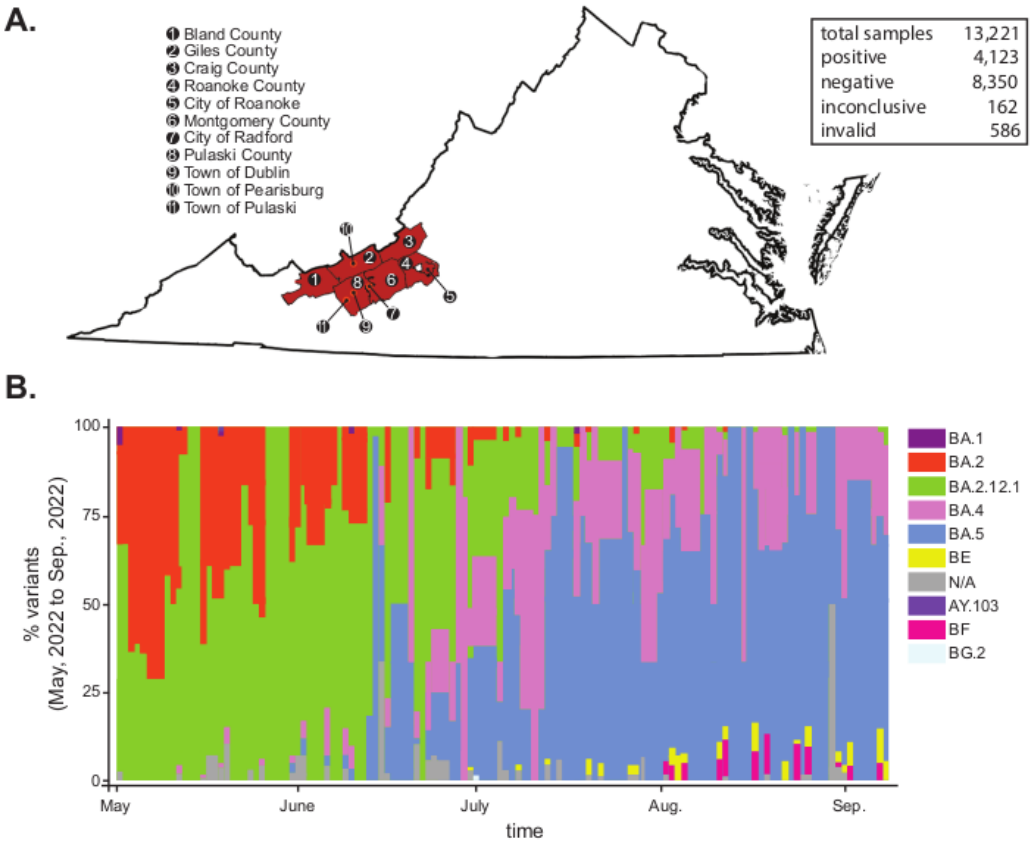

Figure S1. Distribution of SARS-CoV-2 variants in circulation at time of sample collection. (A) Map of counties where sequence data was obtained. (B) Summary of weekly distribution of SARS-CoV-2 variants circulating in human communities in Southwest Virginia between May and September, 2022 as determined by RT-qPCR, RMA, and WGS sequencing.

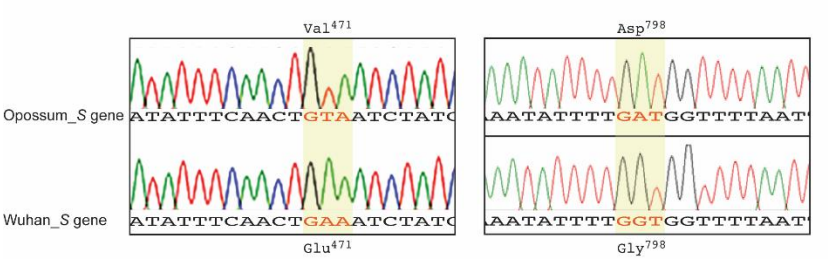

Figure S2. Sanger sequencing peaks of the genomic regions flanking the Glu^{471}Val (left) and Gly^{798}Asp (right) mutations identified in the *S* gene of the opossum-infected SARS-CoV-2 sample and its corresponding sequence in the original Wuhan strain. Nucleotide mutations and matching wild-type sequences are shaded in yellow

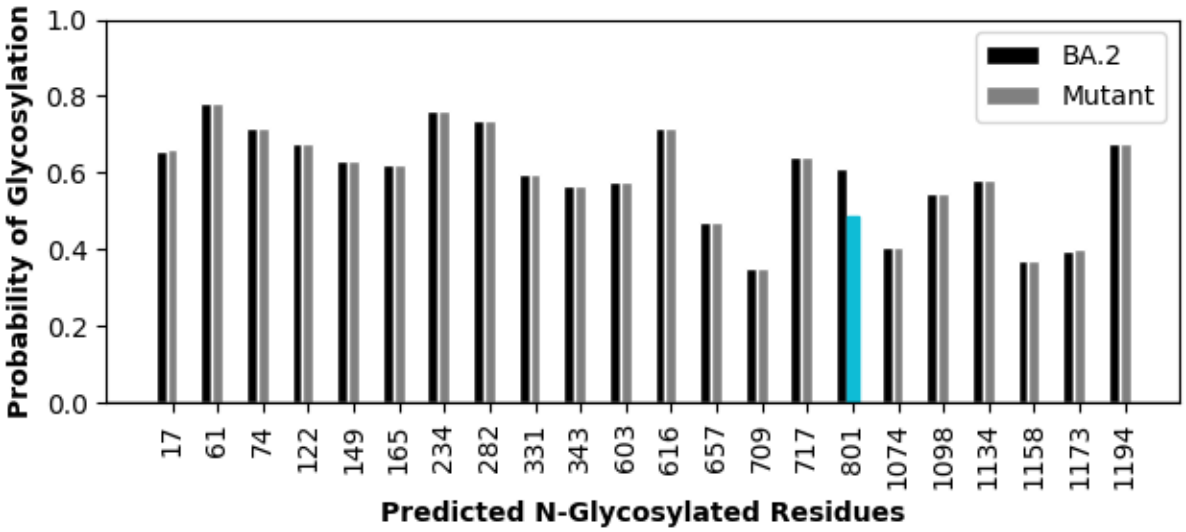

Figure S3. Predicted N-glycosylated residues identified by the NetNGlyc 1.0 server with the probability of being glycosylated based on BA.2 or [mutant] sequence.

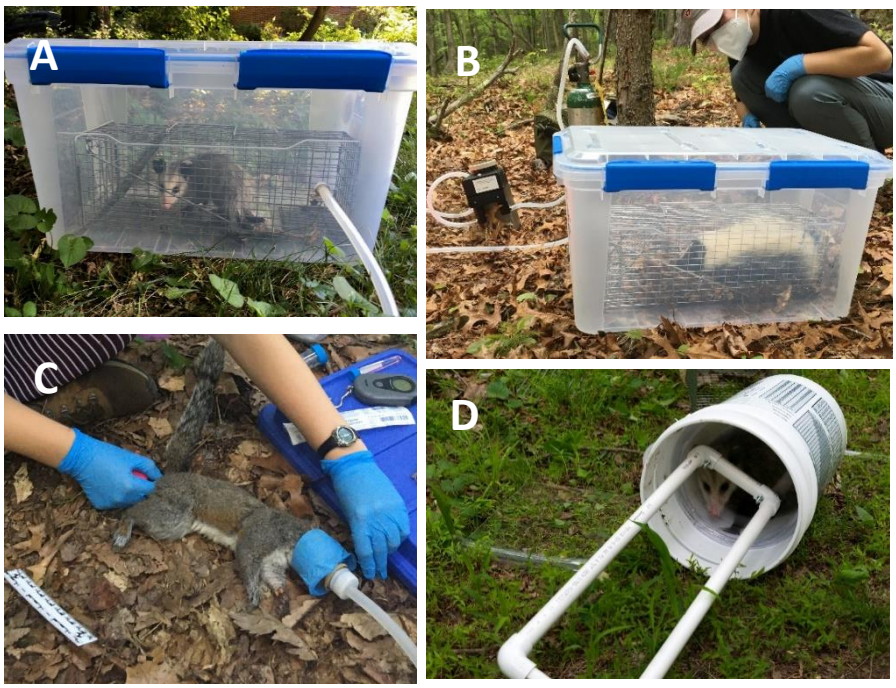

Figure S4. Equipment modified for animal processing. A modified plastic container (A & B). We used a vaporizer with a small O2 tank to supply isoflurane into the chambers (B). We made masks from the top part of a plastic bottle (C). We used a modified bucket chamber for anesthetizing animals trapped in larger cages (D).